Water retained in tall Cryptomeria japonica leaves as studied by infrared micro-spectroscopy

Azuma, Wakana

Nakashima, Satoru

Yamakita, Eri

Ishii, Hiroaki

Kuroda, Keiko

Water retained in tall *Cryptomeria japonica* leaves as studied by infrared micro-spectroscopy

WAKANA AZUMA[1, 3*]

SATORU NAKASHIMA[2]

ERI YAMAKITA[2]

H. ROAKI ISHII[1]

KEIKO KURODA[1]

[1] Graduate School of Agricultural Science, Kobe University, Kobe 675-8501, Japan

[2] Graduate School of Science, Osaka University, Osaka, 560-0043, Japan

[3] Present address: Graduate School of Agriculture, Kyoto University, Kyoto 606-8502, Japan

*Author for correspondence:

Email: wakana@kais.kyoto-u.ac.jp

Phone: +81-75-753-6428

1 **Abstract**

2 Recent studies in the tallest tree species suggest that physiological and anatomical traits of tree-top leaves are

3 adapted to water-limited conditions. In order to examine water retention mechanism of leaves in a tall tree, infrared

4 (IR) micro-spectroscopy was conducted on mature leaf cross-sections of tall *Cryptomeria japonica* from four different

5 heights (51, 43, 31 and 19 m). We measured IR transmission spectra and mainly analyzed OH (3700 – 3000 cm^{-1}) and

6 C-O (1190 – 845 cm^{-1}) absorption bands, indicating water molecules and sugar groups respectively. The changes in IR

7 spectra of leaf sections from different heights were compared with bulk-leaf hydraulics. Both average OH band area of

8 the leaf sections and leaf water content were larger in the upper-crown, while osmotic potential at saturation did not

9 vary with height suggesting higher dissolved sugar contents of upper-crown leaves. As cell-wall is the main cellular

10 structure of leaves, we inferred that larger average C-O band area of upper-crown leaves reflected higher content of

11 structural polysaccharides such as cellulose, hemicellulose, and pectin. IR micro-spectroscopic imaging showed that

12 the OH and C-O band areas are large in the vascular bundle, transfusion tissue, and epidermis. IR spectra of individual

13 tissue showed much more water is retained in vascular bundle and transfusion tissue than mesophyll. These results

14 demonstrate that IR micro-spectroscopy is a powerful tool for visualizing detailed, quantitative information on the

15 spatial distribution of chemical substances within plant tissues, which cannot be done using conventional methods like

16 histochemical staining. The OH band could be well reproduced by four Gaussian OH components around 3530 (free

17 water: long H bond), 3410 (pectin-like OH species), 3310 (cellulose-like OH species) and 3210 (bound water: short H

18 bond) cm^{-1}, and all of these OH components were higher in the upper crown while their relative proportions did not

19 vary with height. Based on the spectral analyses, we inferred that polysaccharides play a key role in biomolecular

20 retention of water in leaves of tall *C. japonica*.

21

22 **Keywords:** water retention; hydrogen bonding; hydraulics; polysaccharides; infrared imaging; Cupressaceae

Introduction

23   Water transport from root to leaf via xylem in tall trees is realized by the gradient of water potential and

24   supports vital metabolisms like photosynthesis and transpiration (Larcher 2003). As trees become tall, a gradient of

25   light and water availabilities is formed within the crown (Koch et al. 2004, Ishii et al. 2008). At the top of tall trees,

26   light availability for photosynthesis is high, but the water availability is physically constrained by long-distance water

27   transport and increasing gravitational potential and hydrodynamic resistance (Ryan and Yoder 1997, Midgley 2003,

28   Franks 2006).

29   In a recent study, it was found that tree-top leaves of the tallest tree species, *Sequoia sempervirens* D. Don

30   (Cupressaceae), have capacity for foliar water storage, which may compensate for constraints on water transport from

31   roots (Ishii et al. 2014). The same mechanism was also found in the tallest tree species in Japan, *Cryptomeria japonica*

32   D. Don (Cupressaceae) (Azuma et al. 2016). In both species, greater water storage capacity of tree-top leaves was

33   associated with larger volume of transfusion tissue, which is gymnosperm-specific conducting tissue surrounding the

34   vascular bundle and has functions in water storage and transportation (Takeda 1931, Hu and Yao 1981, Brodribb et al.

35   2010, Oldham et al. 2010, Aloni et al. 2013, Azuma et al. 2016). These results suggest that anatomical structure of

36   tree-top leaves is adapted to the water-limited conditions. It remains unclear, however, where and how much leaf

37   tissues actually retain water.

38   Here, we used infrared (IR) micro-spectroscopy to investigate anatomical structures in leaves of tall *C.*

39   *japonica* that contribute to water-retention. IR micro-spectroscopy can visualize detailed, quantitative information on

40   where and how much various compounds reside within tissues (Gierlinger and Schwanninger 2007, Fackler et al.

41   2010), which cannot be done using conventional methods such as histochemical staining. IR spectroscopy has been

42   used in plant studies such as plant anatomy, physiology and ecology (Bamba et al. 2002, Dokken et al. 2005, Ribeiro

43   da Luz 2006, Heraud et al. 2007, Martín-Gómez et al. 2015). IR spectroscopy can visualize spatially localized

44   distributions and relative amounts of chemical components within tissues and cells (Dokken and Davis 2007, Heraud

45   et al. 2007). Water molecules are considered to be present in various physicochemical states because of varying

46   hydrogen bond distances among them (Maréchal 2007). In IR spectroscopy, OH stretching absorption frequency is

47   known to decrease with decreasing intermolecular hydrogen bond distance (Nakamoto et al. 1955). Therefore, IR OH

48   bands are used for studying hydrogen bonding nature of water molecules associated with bio-macromolecules. Such

49   physicochemical differences of water molecules are considered to affect physiological functions in living systems

50 (Nakashima et al. 2004, Maréchal 2007). Although hydrogen bonding nature of water molecules may be associated

51 with water retention, it has not been documented in tree leaves. To investigate water retention mechanisms in the

52 leaves of tall *C. japonica*, we measured OH and C-O absorption bands on leaf cross-sections using IR

53 micro-spectroscopy to visualize where and how much water and sugars reside within leaf tissue. Our final goal is to

54 elucidate molecular mechanisms of water retention within leaves. Here, we show initial results of IR

55 micro-spectroscopy in association with physiological measurements of leaf water-relations characteristics to

56 demonstrate application of this new technique to tree ecophysiology research.

57

Material and Methods

58

Sample collection

59

60   A 250-year-old *C. japonica* tree (height = 51 m, diameter at breast height = 114 cm) at Nibuna-Mizusawa

61 Forest Reserve, Tashirozawa National Forest in Akita Prefecture, Japan (40.08°N, 140.25°E, 200 m altitude from sea

62 level) was selected here as a representative tall, mature tree. In November 2013, we accessed the crown of the study

63 tree using single-rope climbing technique. We collected small branches (30−50 cm long) from the outer crown from

64 just below tree-top to the lowest living branches at four different heights (51, 43, 31 and 19 m). Some parts of sample

65 branches were sealed in black plastic bags and stored in a refrigerator for IR micro-spectroscopy and the rest were

66 used soon after sampling for physiological measurements. To quantify the light environment as canopy openness,

67 hemispherical photographs were taken directly above each sampling location and analyzed using Gap Light Analyzer

68 (ver 3.1, Simon Frazer University, Bernaby, BC, Canada). Canopy openness was 19.2 %, 21.8 %, 22.9%, and 83.5% at

69 19 m, 31 m, 43 m, and 51 m, respectively.

70

IR micro-spectroscopy for leaves

71

72   Second-year leaves (mature leaves) were transversely sectioned at the midpoint between leaf tip and its stem

73 attachment to 24 µm thickness using a sliding microtome equipped with frozen mounting device (REM-710, Yamato

74 Kohki Industrial Co., Ltd, Saitama, Japan) (Fig. 1a). Three leaves at each height were sectioned and mounted on an

75 IR-transparent CaF_2 crystal (Fig. 1b).

76   In order to confirm that water in the sectioned leaves was in equilibrium with the room temperature/humidity

77 conditions, transmission IR spectra of a leaf section sampled at 43 m height was measured at intervals of 60 seconds

78   using a Fourier-transform infrared (FT-IR) micro-spectrometer (FTIR-620 + IRT30, Jasco, Tokyo, Japan). A 625 μm×

79   625 μm aperture area in the central part of the leaf cross section (Fig.1 c,d) was monitored with 64 scans at 4 cm^{-1}

80   resolution in the 4000 – 800 cm^{-1} region. Then at 9, 17 and 23 days after sectioning, transmission IR spectra of all leaf

81   sections at four heights were measured using the same FT-IR micro-spectrometer with the same aperture in the central

82   part of leaf cross sections with the same measurement conditions as above. During the measurements, room

83   temperature and humidity were kept constant around 22 ℃ and 35 %, respectively, by air conditioner. IR band area of

84   OH (3700 – 3000 cm^{-1}) and C-O (1190 – 845 cm^{-1}) were measured with baselines set for each band region by Spectra

85   Manager software (Jasco, Tokyo, Japan). We calculated their mean values of three leaf samples for each measurement

86   day.

87   In the interval measurement of transmission IR spectra, OH band area in the sectioned leaves decreased during

88   the first seven hours after sectioning and then became constant. IR spectra of the leaves from four different heights did

89   not show significant changes 9, 17 and 23 days after sectioning, indicating that loss of water from the leaf sections

90   was limited to the first several hours and water contents equilibrated with ambient humidity/temperature thereafter.

91   To measure microscopic distribution of water and polysaccharides over a wider area at higher spatial resolution,

92   IR micro-spectroscopic imaging was also performed on the same leaf sections after 1 day from sectioning using an IR

93   imaging micro-spectrometer (Nicolet iN10MX, Thermo Fisher Scientific, Yokohama, Japan) equipped with a 16

94   channel linear array MCT detector (1 pixel: 25 μm×25 μm). IR spectra were obtained with 1 scan in the 4000 – 800

95   cm^{-1} region at 16 cm^{-1} resolution. IR mapping images of the spatial distribution of band areas and peak height within

96   the leaf cross-sections were generated using OMNIC Spectra Software (Thermo Fisher Scientific, Yokohama, Japan).

97   To quantify IR band areas of leaf tissue, three IR spectra from mesophyll, two IR spectra from transfusion tissue, and

98   one IR spectra from vascular bundle were selected from the IR mapping images using OMNIC Spectra Software

99   (Thermo Fisher Scientific, Yokohama, Japan). Then, IR band area of OH (3700 – 3000 cm^{-1}) and C-O (1190 – 845

100 cm^{-1}) of each tissue were measured using Spectra Manager software (Jasco, Tokyo, Japan).

101

Identifying OH and C-O band species correlated with water retention

103   The IR spectrum of the leaf section at 19 m height was subtracted from those at 51, 43 and 31 m heights to

104 discriminate different water and polysaccharide species at different heights. To normalize spectra among different

105 heights, the 19-m spectrum was multiplied by a coefficient (1.98, 1.20, and 1.33 for 51, 43, and 31 m, respectively),

106 which was derived so that the difference spectra at 3000 cm^{-1} (which is considered as the stable absorption minimum)

107 between 19 m and each height is zero. In the OH stretching region, positive bands at *c.* 3520 cm^{-1} and *c.* 3250 cm^{-1}

108 were observed (Fig. 2b). These bands were higher for upper-crown leaves.

109   In IR spectroscopy, there is a large body of literature indicating strong correlations between CO, OH band

110 areas and carbohydrate, water contents, respectively (e.g. Liang and Marchessault 1959, Olsson and Salmén 2004,

111 Mayers et al. 2013, Kudo et al. 2017). Cellulose and pectin are two major polysaccharides in leaf tissues. To examine

112 OH bands of cellulose and pectin, 0.5 wt. % cellulose and pectin pellets were prepared from cellulose powder (CAS

113 No. 9004-34-6, Wako Pure Chemical Industries. Ltd.) and pectin powder (CAS No 9000-69-5, Wako Pure Chemical

114 Industries. Ltd.) by the KBr pellets method (Smith 2011, Tonoue et al. 2014), for measuring IR transmission spectra

115 with the same conditions as the measurement of transverse sectioned leaf using Jasco's FT-IR micro-spectrometer. The

116 3310 cm^{-1} band is considered to be from OH groups in cellulose, while the 3410 cm^{-1} band is from –COOH groups in

117 pectin (Fig. 2c). As the OH band positions observed in the difference spectra of leaves (3520, 3250 cm^{-1}) and in the

118 cellulose and pectin films (3310, 3410 cm^{-1}) were considered to be a representative OH band components of leaves,

119 they were used as fixed positions for fitting the OH bands of leaves by four Gaussian bands to compare compositions

120 of OH species among different heights/tissues. IR spectra of sectioned leaves were compared with those of cellulose

121 and pectin for C-O absorption bands in the 1800 – 1000 cm^{-1}.

122

Relationship between OH band area and amount of water

124   To test the relationship between increasing OH band area and amount of water, IR spectrum and weight

125 changes of water adsorption/desorption of a pectin film was measured simultaneously using the same FT-IR

126 micro-spectroscopy as leaf samples and Quartz crystal microbalance (QCM-30L, SEIKO EG&G, Tokyo, Japan) under

127 controlled relative humidity (RH, %) following methods described in Kudo et al. (2017). Pectin film was made from

128 0.3 wt. % pectin solution. We measured the IR spectra and weights of pectin film at RH = around 20, 30, 40, 50, 60 %,

129 and then calculated the change in OH band area (3700 – 3000 cm^{-1}) and amount of water (μg) with the change in RH.

130   With increasing water adsorbed on pectin film under controlled relative humidity, the OH band area increased

131 linearly (Fig 2, $R^2 = 0.99$, $P < 0.001$). These correlations support that (1) OH band area in IR spectra of leaves can be a

132 good indicator of water retained in leaf tissues such as pectin and (2) water represented by the OH band area is

133 associated with polysaccharides represented by CO band area.

134

Physiological measurement of leaf hydraulics

136　　　To compare the results of IR micro-spectroscopy with physiological measurements, five or six shoots

137　comprising second- and current-year internodes were removed from sampled branches at each height for measurement

138　of bulk leaf hydraulic properties as described in Azuma et al. (2016). Briefly, osmotic potentials at saturation (Ψ_{sat},

139　MPa), osmotic potential at turgor loss (Ψ_{tlp}, MPa), relative water content at turgor loss (RWC_{tlp}), and leaf capacitance

140　(C_{leaf}, mol m^{-2} MPa^{-1}) were obtained from the pressure-volume curve using the bench drying approach (Tyree and

141　Hammel 1972, Schulte and Hinckley 1985, Azuma et al. 2016) with a pressure chamber (Model 1000, PMS

142　Instruments, Corvallis, OR,USA). Then, all the sample shoots were photographed for measurement of leaf surface

143　area. The saturated leaf water content (WW, g) was calculated by subtracting the dry weight, after drying to constant

144　weight at 65 ℃, from the fresh leaf weight at water saturation. Leaf dry weights were normalized by the leaf surface

145　area to obtain saturated leaf water content per unit area or succulence (S_{leaf}, g H_2O m^{-2}; Bacelar et al. 2004, Ishii et al.

146　2014, Azuma et al. 2016).

147

Data analyses

149　　　　We compared the effects of light environment (O_c, log transformed canopy openness) to normalize the

150　variance) and height on IR spectra and bulk-leaf hydraulics using regression analysis, following the methods described

151　in Coble and Cavaleri (2015). To compare IR measurements and physiological measurements, OH and C-O of IR band

152　area were analyzed in relation to bulk-leaf hydraulics using regression analysis. OH and C-O band areas were

153　compared among leaf tissue (mesophyll, transfusion tissue, and vascular bundle) using Tukey's HSD test (p <0.05)

154　after regression analysis against height for each tissue. Compositions of OH species among 3530, 3410, 3210 and

155　3310 cm^{-1} were compared among leaf tissue using Tukey's HSD test (p <0.05) after regression analysis against height

156　for each OH species.

157

Results

159　　　Fig. 3a shows IR absorbance spectra of the leaf at 51, 43, 31 and 19 m height 23 days after sectioning.

160　Although IR spectra were measured in the 4000 – 800 cm^{-1} range, data below 900 cm^{-1} are not shown in Fig.3 due to

161　low signals by CaF$_2$ window cutoff. The broad band *c.* 3325 cm^{-1} is due to OH stretching vibrations. The band with

162 peaks at 2920 and 2855 cm^{-1} are asymmetric and symmetric stretching of aliphatic CH_2. The band at *c.* 1740 cm^{-1} is

163 C=O stretching of carboxyl (COOH). The band at 1640 cm^{-1} is bending mode of water molecules. The shoulder *c.*

164 1645 cm^{-1} could have originated from amide I (C=O stretching) of proteins. The band *c.* 1610 cm^{-1} could be due to

165 COO⁻ species (deprotonated COOH). The small band *c.* 1545 cm^{-1} might be amide II (C-N-H bending, C-N stretching

166 of peptides). The band at 1415 cm^{-1} could have originated from COO⁻ of pectin and that at 1370 cm^{-1} band is due to

167 bending of aliphatic CHs. The 1320 cm^{-1} and 1235 cm^{-1} band corresponds to amide III (C-N-H bending, C-N

168 stretching of peptides). The small band at 1315 cm^{-1} could be from OH bending in plane of alcohol group. The strong

169 band at *c.* 1020 cm^{-1} is due to C-O species in polysaccharides. The assignments of these bands are summarized in

170 Table 1.

171   When the IR spectra of sectioned leaves (Fig. 3a) was compared to that of the pectin and cellulose (Fig. 3b),

172 the bands in the 1800 – 1000 cm^{-1}, in particular *c.* 1735 cm^{-1} (COOH) and 1610 cm^{-1} (COO⁻), were similar to those for

173 pectin but the correspondence was not clear for cellulose. In the 1800 – 1000 cm^{-1} region of the difference spectra

174 from the leaf at 19 m height (Fig.3c), several positive bands are observed. The positive bands that are higher for

175 upper-crown leaves include contributions mainly from 1) amide I (1670 cm^{-1}) and II (1550 cm^{-1}) bands of proteins

176 present in mesophyll (possibly photosynthetic protein such as Rubisco), 2) COO⁻ of pectin (1415 cm^{-1}), and 3) C-O-C

177 (1170 and 1120 cm^{-1}) of polysaccharides.

178

IR spectra and IR maps of leaf sections from different heights

180   OH (3700 – 3000 cm^{-1}) and C-O (1800 – 845 cm^{-1}) band areas were positively correlated with both light (O_c)

181 and height. OH band area was more affected by light than height, while CO band area was more affected by height

182 (Table 2). OH and C-O band areas were positively correlated with each other (Fig. 4, $R^2 = 0.54$, $P < 0.001$).

183   IR micro-spectroscopic imaging allowed visualization of the spatial distribution of absorption bands within

184 leaf sections (Fig. 5). In the leaf at 19 m height, OH band area (3700 – 3000 cm^{-1}) was large in the center of the leaf,

185 corresponding to the vascular bundle and transfusion tissue, and in epidermis (red portions in Fig. 5a). Although the

186 leaves at 31 and 43 m showed similar distribution patterns as leaves at 19m, the image of leaves at 51 m indicated

187 large band areas in the mesophyll regions. C-O band area (1190 – 845 cm^{-1}) in the leaf at 19 m was large around

188 vascular bundle, transfusion tissue, and epidermis (red portions in Fig. 5b). At 31 and 43 m, the region of large C-O

189 band area included mesophyll around the leaf periphery, and at 51 m, was widespread in all areas of the leaf. The

190 observed height-related patterns in OH and C-O band areas within leaf tissue explain well, the results shown in Table

191 2 and Fig. 4. For C-O-C bands, the ratio of 1120 cm^{-1} for 1170 cm^{-1} of polysaccharides was higher in upper-crown

192 leaves around the vascular bundle and transfusion tissue (Fig. 5c).   We discuss what it means in the Discussion part

193 in relation to C-O band species.

194   A fitting result of four representative OH band components of leaves is shown in Fig. 6a. Average band areas

195 of the four Gaussian components for three samples at each height was highest in the tree-top leaves (Fig. 6b). On the

196 other hand, band area ratios did not vary with height (Fig. 6c). The band area of c. 3410 cm^{-1} (–COOH groups in

197 pectin-like species) and c. 3210 cm^{-1} (water molecules with shorter H bonds) components occupy about 30%,

198 respectively, and those of c. 3530 cm^{-1} (water molecules with longer H bonds) and c. 3310 cm^{-1} (OH groups in

199 cellulose-like species) occupy about 20%, respectively, suggesting bound water might be more abundant than free

200 water.

201

Selected IR spectra in mesophyll, transfusion tissue, and vascular

203   Figure 7 shows the average OH and C-O band areas of mesophyll, transfusion tissue, and vascular bundle from

204 different heights (n = 3, 2, and 1, respectively at each height). For each tissue, both band areas show no systematic

205 trends with height. Both band areas were largest in vascular bundle, followed by transfusion tissue and smallest in

206 mesophyll.

207   Figure 8 shows the percentages of average band area ratios of mesophyll, transfusion tissue and vascular

208 bundle (n = 3, 2 and 1 at each height, respectively) as the fitting results of representative OH band components. For

209 each OH band components, the average band area ratios show no systematic trends with height. The band area of c.

210 3410 cm^{-1} (–COOH groups in pectin-like species) was the most abundant component in each tissue, especially in

211 mesophyll.

212

Bulk-leaf hydraulics

214   With the exception of $\varPsi_{sat}$ and $\varPsi_{tlp}$, bulk-leaf hydraulic properties were correlated with both light (O_c) and

215 height (Table 2). RWC$_{tlp}$, WW, and S_{leaf} were more affected by light, while C_{leaf} was more affected by height. Bulk-leaf

216 hydraulic properties, except for $\varPsi_{sat}$, $\varPsi_{tlp}$, and S_{leaf}, were correlated with average OH and C-O band areas (Table 3).

217 WW was correlated with both OH and C-O band areas, while C_{leaf} and RWC$_{tlp}$ were correlated with C-O band area.

218

219

Discussion

221   Our study demonstrated that IR micro-spectroscopy is a powerful tool for visualizing detailed spatial

222 distribution of chemical substances within plant tissue. IR spectroscopy has been used for investigating hydrogen

223 bonding in complex organic polymers such as lignin, cellulose, and hemi cellulose (e.g. Maréchal and Chanzy 2000,

224 Olsson and Salmén 2004, Kubo and Kadla 2005, Fackler et al. 2010). While we could not elucidate how water is

225 bound to mixed polymers within leaves, the observed height-related pattern of spatial correlation between OH and

226 C-O band areas within leaf tissue (Figs. 4 and 5), suggest polysaccharides may contribute to water retention in tree-top

227 leaves. Osmotic regulation in leaves is considered to be controlled mainly by dissolved sugars in plant cells (Ackerson

228 1981, Watanabe et al. 2000). In this study, osmotic potential of saturated leaves did not change with height, suggested

229 larger amounts of dissolved sugars in the tree-top leaves, which have higher leaf water contents. Constant osmotic

230 potential of saturated leaves within crown was observed during bud break in May (Azuma et al. 2016) and late season

231 in November in this study, suggested it could be regular bulk-leaf hydraulics through the year in tall *C. japonica*. The

232 IR spectra of $1800 - 1000$ cm^{-1} region suggested that sectioned leaves contained polysaccharides, in particular

233 pectin-like materials. Plant cell-walls consist of structural polysaccharides such as cellulose, hemicellulose and pectin

234 whose proportions change for different species (Evert 2006, Fukushima et al. 2011). These polysaccharides are the

235 main substances of the cellular framework. We postulate that, in the case of very thinly sliced leaves equilibrated with

236 the ambient environmental humidity, water molecules are retained in microstructures of the cellular framework

237 containing polysaccharides.

238   The results of correlations among OH band area and bulk-leaf hydraulics suggested that OH band area of IR

239 spectrum reflected amount of water in cross-sectioned leaves, but there were no clear relationships with some

240 measures such as Ψ_{tlp} and C_{leaf}. In tall trees, leaf hydraulics change in response to the vertical gradients of water

241 potential, which is determined by both height via hydrostatic gradient and light via evaporative demand (Ryan and

242 Yoder 1997, Koch et al. 2004). We found, in tall *C. japonica*, measures of water retention and storage (OH band area,

243 RWC$_{tlp}$, WW, and S_{leaf}) were more affected by light than height. This may reflect physiological adaptation for

244 maintaining leaf water status near the tree top, where the light environment is favorable for photosynthesis.

245 Correlations of C-O band area with RWC$_{tlp}$, C_{leaf}, and WW suggest that some sugar species may be involved in

246   determining leaf hydraulic properties. Both C-O band area and C_{leaf} were more affected by height than light,

247   suggesting physiological adaptation to the hydrostatic gradient of water potential may be achieved by increasing

248   non-structural carbohydrate concentration in leaves.

249   Bamba et al. (2002) investigated the localization of polyisoprene in young stem tissues of *Eucommia ulmoides*

250   Oliver using histochemical staining and IR micro-spectroscopy. They showed by IR micro-spectroscopy the

251   localization and accumulation of polyisoprene in plant tissue. In our study, while conventional dye staining method

252   (e.g., PAS staining) to visualize polysaccharides on the present leaves showed global pink coloration of the entire leaf

253   (data not shown), IR mapping of C-O band area showed localization of polysaccharides as well as quantitative

254   information of their relative concentrations. In addition to visualization within cross-sectioned leaf in IR maps,

255   selected IR spectra of individual tissue showed characteristic chemical compositions of individual tissue. Among the

256   three main water-related leaf tissues (mesophyll, transfusion tissue and vascular bundle), our results indicated much

257   more water is retained in vascular bundle than mesophyll. The water storing function of transfusion tissue acts as a

258   hydraulic buffer in leaves of tall *C. japonica* preventing excessive decrease in xylem water potential (Azuma et al.

259   2016). Here, we showed more water is retained in transfusion tissue than mesophyll. Such a gradient in water retention

260   capacity from sink to source may function to maintain hydraulic safety of water transport within leaves.

261   Since pectin-like OH species is the major component particularly in mesophyll, pectin may contribute to water

262   retention in thin cell walls and large cytoplasm of mesophyll, in contrast to thick cell walls and small conduits of

263   vascular xylem and transfusion tissue. In a recent novel study, Bouche et al. (2016) conducted visual quantification of

264   hydraulic failure in leaf and stem tissues to test the vulnerability segmentation hypothesis using high-resolution

265   computed tomography, and suggested the importance of imaging techniques for vulnerability curves. Quantitative

266   visualization of plant functional traits conducted in conjunction with measurements of dynamic, physiological

267   responses and micro-scale anatomical structure are thus expected to provide effective new ways to study plant

268   physiology.

269

270   *Biomolecules relating to water retention*

271   Based on inferences made by examining which OH band components are present in the OH stretching region,

272   we present a hypothesis for biomolecular retention of water in leaves. The amount of water retained in leaves was

273   greater for tree-top leaves, but the water species seems to be similar among different heights, indicating that

274   physicochemical traits of water does not change with height. This suggests higher content of water-retaining

275   substances such as pectin- and cellulose-like compounds in tree-top leaves Considering the main C-O species detected

276   from the difference spectra, higher content of proteins in upper-crown leaves is likely to reflect high-light acclimation

277   for increasing photosynthetic proteins such as Rubisco (Warren and Adams 2001). The increase of COO^- possibly

278   linked to pectin in the tree-top leaves can be explained by decarboxylation of –COOH and its binding to Ca^{2+} in the

279   cell forming $Ca^{2+} - {}^-OOC$ linkage for cell walls of leaf tissue (Demarty et al. 1984, Liners et al. 1989, Dunand et al.

280   2002). The presence of positive bands from 1740 to 1610 cm^{-1} (Fig.2c) can also be explained by this conversion of

281   COOH (1740 cm^{-1}) to COO^- (1610 cm^{-1}). The IR maps showed, for C-O-C bands, the ratio of two bands (1120 cm^{-1}

282   for 1170 cm^{-1}) of polysaccharides was higher in upper-crown leaves around the vascular bundle and transfusion tissue

283   (Fig. 5c). On the other hand, amounts of water and polysaccharides were greater in peripheral regions of mesophyll

284   (Fig. 5a, b). The band around 1145 cm^{-1} for pectin (Fig.2b) can be shifted to the lower wavenumber region by

285   hydrogen bonding of adsorbed water molecules to C-O species. Therefore, the increase in the ratio of 1120 cm^{-1} for

286   1170 cm^{-1} with height for mesophyll regions in the IR map (Fig. 5c) can be tentatively explained by a shift of C-O

287   bonds by hydrogen bonding to water molecules. Thus, some changes in polysaccharides might be related to the

288   effective radial transport and retention of water in tree-top leaves although its origin remains unknown.

289   As described above, Ca^{2+} ions are known to bond to deprotonated carboxyl groups (COO–) (e.g., in pectin) to

290   form Ca bridges linking polysaccharide molecules in plant cell wall (Fig 9a, Demarty et al. 1984, Liners et al. 1989,

291   Dunand et al. 2002). If polysaccharides are involved in water retention in leaves, one possible mechanism could be

292   that water molecules are bound to the Ca-linked pectin molecules by hydrogen bonding to C-O-C and C-OH (Fig. 9b).

293   Although further detailed studies for water adsorption by polysaccharides (pectin, cellulose, hemi-cellulose), lignin,

294   proteins such as Rubisco, and lipids in leaves are needed, our observation of higher polysaccharide content in tree-top

295   leaves suggest that a similar mechanism could explain water retention in leaves of tall trees.

296

Physiological significance of water retention in tall trees

298   In tall trees, water transport from root to tree-top is necessary for photosynthesis, and ultimately for tree

299   growth and survival, but becomes physically difficult with increasing height. To overcome this constraint, stored

300   water could help alleviate water stress in tree top leaves, especially if it is easily readily accessible. In *Pseudotsuga*

301   *menziesii* (Mirb.) Franco var. *menziesii*, it is suggested that stem water storage plays a significant role in the water

302 economy with increasing tree size and helps to maintain whole trees transpiration (Phillips et al. 2003, Cermák et al.

303 2007). Among canopy trees in Hawaiian dry forest, stem water storage capacity was positively correlated with water

304 transport efficiency (Stratton et al. 2000). In *S. sempervirens* and *C. japonica*, an larger amounts of stored water in

305 leaves compensate severe water stress at tree-top (Ishii et al. 2014, Azuma et al. 2016). In young *Picea abies* L.,

306 stored water contributes to 10% and 65% of daily transpiration on sunny and cloudy days, respectively (Zweifel et al.

307 2001). In young *C. japonica,* stored water contributes to 10% of total daily transpiration on sunny day, more than half

308 of which is stored in leaves (Himeno et al. in press). These studies suggest that stored water in stem and leaves play a

309 significant role for maintaining physiological function in trees. Our results showing greater water retention in

310 tree-top leaves of tall *C. japonica*, which are in favorable light environment give additional support to physiological

311 acclimation of leaves to increasing height in tall trees. A novel finding of this study is that polysaccharides may be

312 associated with water retention in leaves.

313

Future issues

315 In this study, we focused on OH absorption bands in IR spectra of cross-sectioned leaves and analyses of the

316 detailed OH band species characteristics. The results of four OH components at different heights and tissue suggested

317 that some changes in polysaccharides might be related to the effective radial transport and retention of water. To

318 explain the relationship between hydrogen bonding and sugar species, we need to seek individual sugar species from

319 C-O absorption band and investigate what C-O band species are correlated with OH band species. It is also necessary

320 to investigate the correlation of IR bands with conventional chemical carbohydrate analyses of bulk-leaf for individual

321 polysaccharides. In addition to osmotic regulation by dissolved sugars, water may also be bound in microstructures of

322 the cellular framework involving Ca bridges linking pectin chains, one possible mechanism for water retention within

323 leaves. The role of bound water in plant physiology may be elucidated by focusing on physicochemical traits of

324 retained and transported water in future studies.

325

330 Univ. for field assistance and Drs. A. Makita, K. Takata, K. Hoshizaki, and M. Matsushita of Akita Pref. Univ. for

331 facilitating the study.

332

335

336 **References**

337 Ackerson RC (1981) Osmoregulation in cotton in response to water stress : II. Leaf carbohydrate status in relation to

338   osmotic adjustment. Plant Physiol 67:489–493.

339 Aloni R, Foster A, Mattsson J (2013) Transfusion tracheids in the conifer leaves of *Thuja plicata* (Cupressaceae) are

340   derived from parenchyma and their differentiation is induced by auxin. Am J Bot 100:1949–1956.

341 Azuma W, Ishii HR, Kuroda K, Kuroda K (2016) Function and structure of leaves contributing to increasing water

342   storage with height in the tallest *Cryptomeria japonica* trees of Japan. Trees 30:141–152.

343 Bacelar EA, Correia CM, Moutinho-Pereira JM, Goncalves BC, Lopes JI, Torres-Pereira JMG (2004) Sclerophylly

344   and leaf anatomical traits of five field-grown olive cultivars growing under drought conditions. Tree Physiol

345   24:233–239.

346 Bamba T, Fukusaki EI, Nakazawa Y, Kobayashi A (2002) In-situ chemical analyses of trans-polyisoprene by

347   histochemical staining and Fourier transform infrared microspectroscopy in a rubber-producing plant, Eucommia

348   ulmoides Oliver. Planta 215:934–939.

349 Bouche PS, Delzon S, Choat B, Badel E, Brodribb TJ, Burlett R, Cochard H, Charra-Vaskou K, Lavigne B, Li S,

350   Mayr S, Morris H, Torres-Ruiz JM, Zufferey V, Jansen S (2016) Are needles of *Pinus pinaster* more vulnerable

351   to xylem embolism than branches? New insights from X-ray computed tomography. Plant, Cell Environ 39:

352   860-870.

353 Brodribb TJ, Feild TS, Sack L (2010) Viewing leaf structure and evolution from a hydraulic perspective. Funct Plant

354   Biol 37:488–498.

355 Cermák J, Kucera J, Bauerle WL, Phillips N, Hinckley TM, Cermak J, Kucera J, Bauerle WL, Phillips N, Hinckley

356   TM (2007) Tree water storage and its diurnal dynamics related to sap flow and changes in stem volume in

357   old-growth Douglas-fir trees. Tree Physiol 27:181–198.

358   Demarty M, Morvan C, Thellier M (1984) Calcium and the cell wall. Plant, Cell Environ 7:441–448.

359   Dokken KM, Davis LC (2007) Infrared imaging of sunflower and maize root anatomy. J Agric Food Chem 55:10517–

360   10530.

361   Dokken KM, Davis LC, Marinkovic NS (2005) Use of infrared microspectroscopy in plant growth and development.

362   Appl Spectrosc Rev 40:301–326.

363   Dunand C, Tognolli M, Overney S, Tobel L Von, Meyer M De, Simon P, Penel C (2002) Identification and

364   characterisation of Ca^{2+}-pectate binding peroxidases in *Arabidopsis thaliana*. J Plant Physiol 1171:0–6.

365   Evert RF (2006) Esau's plant anatomy: meristems, cells, and tissues of the plant body: their structure, function, and

366   development. John Wiley & Sons, New Jersey.

367   Fabian H, Naumann D (2012) Millisecond-to-minute protein folding/misfolding events monitored by FTIR

368   spectroscopy. In: Fabian H, Naumann D (eds) Protein folding and misfolding. Springer, Berlin, pp 53–89.

369   Fackler K, Stevanic JS, Ters T, Hinterstoisser B, Schwanninger M, Salmén L (2010) Localisation and characterisation

370   of incipient brown-rot decay within spruce wood cell walls using FT-IR imaging microscopy. Enzyme Microb

371   Technol 47:257–267.

372   Franks PJ (2006) Higher rates of leaf gas exchange are associated with higher leaf hydrodynamic pressure gradients.

373   Plant, Cell Environ 29:584–592.

374   Fukushima K, Funada R, Sugiyama J, Takabe K, Umezawa T, Yamamoto H (eds) (2011) Secondary xylem

375   formation-Introduction to biomass science-2nd edition. Kaiseisha Press, Japan.

376   Heraud P, Caine S, Sanson G, Gleadow R, Wood BR, McNaughton D (2007) Focal plane array infrared imaging: a

377   new way to analyse leaf tissue. New Phytol 173:216–225.

378   Gierlinger N, Schwanninger M (2007) The potential of Raman microscopy and Raman imaging in plant research.

379   Spectroscopy 21:69–89.

380   Heraud P, Caine S, Sanson G, Gleadow R, Wood BR, McNaughton D (2007) Focal plane array infrared imaging: a

381   new way to analyse leaf tissue. New Phytol 173:216–225.

382   Hu YS, Yao BJ (1981) Transfusion tissue in gymnosperm leaves. Bot J Linn Soc 83:263–272.

383   Ishii HR, Azuma W, Kuroda K, Sillett SC (2014) Pushing the limits to tree height: could foliar water storage

384   compensate for hydraulic constraints in *Sequoia sempervirens*? Funct Ecol 28:1087–1093.

385   Ishii H, Jennings G, Sillett S, Koch G (2008) Hydrostatic constraints on morphological exploitation of light in tall

386   *Sequoia sempervirens* trees. Oecologia 156:751–763.

387   Kačuráková M, Wellner N, Ebringerová a, Hromádková Z, Wilson R., Belton P. (1999) Characterisation of

388   xylan-type polysaccharides and associated cell wall components by FT-IR and FT-Raman spectroscopies. Food

389   Hydrocoll 13:35–41.

390   Kačuráková M, Wilson RH (2001) Developments in mid-infrared FT-IR spectroscopy of selected carbohydrates.

391   Carbohydr Polym 44:291–303.

392   Koch GW, Sillett SC, Jennings GM, Davis SD (2004) The limits to tree height. Nature 428:851–854.

393   Kubo S, Kadla JF (2005) Hydrogen bonding in lignin: A fourier transform infrared model compound study.

394   Biomacromolecules 6:2815–2821.

395   Kudo S, Ogawa H, Yamakita E, Watanabe S, Suzuki T, Nakashima S (2017) Adsorption of water to collagen as

396   studied using infrared (IR) microscopy combined with relative humidity control system and quartz crystal

397   microbalance. Appl Spectrosc. doi: 10.1177/0003702817693855

398   Labbé N, Rials T, Kelley S, Cheng ZM, Kim JY, Li Y (2005) FT-IR imaging and pyrolysis-molecular beam mass

399   spectrometry: New tools to investigate wood tissues. Wood Sci Technol 39:61–77.

400   Larcher W (2003) Physiological plant ecology: ecophysiology and stress physiology of functional groups. Springer,

401   Berlin.

402   Liang CY, Marchessault RH (1959) Infrared spectra of crystalline polysaccharides. II. Native celluloses in the region

403   from 640 to 1700 cm^{-1}. J Polym Sci 39:269–278.

404   Liners F, Letesson JJ, Didembourg C, Van Cutsem P (1989) Monoclonal antibodies against pectin: recognition of a

405   conformation induced by calcium. Plant Physiol 91:1419–1424.

406   Maréchal Y (2007) The hydrogen bond and the water molecule: The physics and chemistry of water, aqueous and bio

407   media. Elsevier, Netherlands.

408   Maréchal Y, Chanzy H (2000) The hydrogen bond network in I(β) cellulose as observed by infrared spectrometry. J

409   Mol Struct 523:183–196.

410   Martín-Gómez P, Barbeta A, Voltas J, Peñuelas J, Dennis K, Palacio S, Dawson TE, Ferrio JP (2015) Isotope-ratio

411   infrared spectroscopy: a reliable tool for the investigation of plant-water sources? New Phytol 207:914–927.

412   Mayers J, Flynn KJ, Shields RJ, Mayers JJ, Flynn KJ, Shields RJ (2013) Rapid determination of bulk microalgal

413   biochemical composition by Fourier-Transform Infrared spectroscopy. Bioresour Technol 148:215–220.

414   Midgley JJ (2003) Is bigger better in plants? The hydraulic costs of increasing size in trees. Trends Ecol Evol 18:5–6.

415   Nakamoto K, Margoshes M, Rundle RE (1955) Stretching frequencies as a function of distances in hydrogen bonds. J

416   Am Chem Soc 77:6480–6486.

417   Nakashima S, Spiers C., Mercury L, Fenter P., Hochella M. (eds) (2003) Physicochemistry of water in geological and

418   biological systems-Structures and properties of thin aqueous films. Universal Academy Press, Inc., Tokyo,

419   Japan.

420   Oldham AR, Sillett SC, Tomescu AMF, Koch GW (2010) The hydrostatic gradient, not light availability, drives

421   height-related variation in *Sequoia sempervirens* (Cupressaceae) leaf anatomy. Am J Bot 97:1087–1097.

422   Olsson AM, Salmén L (2004) The association of water to cellulose and hemicellulose in paper examined by FTIR

423   spectroscopy. Carbohydr Res 339:813–818.

424   Painter P, Snyder R, Starsinic M, Coleman M, Kuehn D, Davis A (1981) Concerning the application of FT-IR to the

425   study of coal: A critical assessment of band assignments and the application of spectral analysis programs. Appl

426   Spectrosc 35:475–485.

427   Phillips, Ryan MG, Bond BJ, McDowell NG, Hinckley TM, Cermak J (2003) Reliance on stored water increases with

428   tree size in three species in the Pacific Northwest. Tree Physiol 23:237–245.

429   Ribeiro da Luz B (2006) Attenuated total reflectance spectroscopy of plant leaves: A tool for ecological and botanical

430   studies. New Phytol 172:305–318.

431   Ryan MG, Yoder BJ (1997) Hydraulic limits to tree height and tree growth: what keeps trees from growing beyond a

432   certain height? Bioscience 47:235–242.

433   Schulte PJ, Hinckley TM (1985) A comparison of pressure-volume curve data analysis techniques. J Exp Bot

434   36:1590–1602.

435   Smith BC (2011) Fundamentals of Fourier transform infrared spectroscopy Smith BC (ed), 2nd edn. CRC Press,

436   Taylor & Francis Group.

437   Stratton L, Goldstein G, Meinzer FC (2000) Stem water storage capacity and efficiency of water transport: their

438   functional significance in a Hawaiian dry forest. Plant Cell Environ 23:99–106.

439   Synytsya A, Copikova J, Matejka P, Machovic V (2003) Fourier transform Raman and infrared spectroscopy of

440   pectins. Carbohydr Polym 54:97–106.

441   Szymanska-Chargot M, Zdunek A (2013) Use of FT-IR Spectra and PCA to the Bulk Characterization of Cell Wall

442   Residues of Fruits and Vegetables Along a Fraction Process. Food Biophys 8:29–42.

443   Takeda H (1931) A theory of 'transfusion-tissue'. Ann Bot os-27:359–363.

444   Tonoue R, Katsura M, Hamamoto M, Bessho H, Nakashima S (2014) A method to obtain the absorption coefficient

445   spectrum of single grain coal in the aliphatic C-H stretching region using infrared transflection

446   microspectroscopy. Appl Spectrosc 68:733–739.

447   Tyree MT, Hammel HT (1972) The measurement of the turgor pressure and the water relations of plants by the

448   pressure-bomb technique. J Exp Bot 23:267–282.

449   Warren CR, Adams M a. (2001) Distribution of N, Rubisco and photosynthesis in *Pinus pinaster* and acclimation to

450   light. Plant, Cell Environ 24:597–609.

451   Watanabe S, Kojima K, Ide Y, Sasaki S (2000) Effects of saline and osmotic stress on proline and sugar accumulation

452   in *Populus euphratica* in vitro. Plant Cell Tissue Organ Cult 63:199–206.

453   Yang H, Yan R, Chen H, Lee DH, Zheng C (2007) Characteristics of hemicellulose, cellulose and lignin pyrolysis.

454   Fuel 86:1781–1788.

455   Zweifel R, Hasler R (2001) Dynamics of water storage in mature subalpine *Picea abies*: temporal and spatial patterns

456   of change in stem radius. Tree Physiol 21:561–569.

457   Zweifel R, Item H, Häsler R (2001) Link between diurnal stem radius changes and tree water relations. Tree Physiol

458   21:869–877.

459

460

461   **Figure legends**

462   Fig. 1 Procedures for IR micro-spectroscopy of *Cryptomeria japonica* leaves.

463   (a) Sampling and transverse sectioning of leaves. b) Mounting of sections on CaF_2. (c) A microphoto of a

464   transvers section. (d) A magnified central area of 625x625 μm^2 used for IR measurement.

465   Fig. 2 Correlation between increase in amount of water (weight increase: μg) by quartz crystal microbalance and

466   increase in IR OH band area on a pectin film with increasing relative humidity (RH) from 20 to 30, 40, 50 and

467   60 %.

468   Fig. 3 (a) IR absorbance spectra of the leaves at 19, 31, 43 and 51 m, 23 days after sectioning. (b) IR absorbance

469   spectra of cellulose and pectin powders by KBr pellet method. (c) Difference spectra from the 19 m spectrum

470   with a coefficient so as to obtain the absorbance zero at 3000 cm^{-1} (51m spectrum: 51 m – 19 m x 1.98, 43 m:

471   43 m – 19 m x 1.2, 31 m: 31 m – 19 m x1.33) to discriminate water and polysaccharide species at different

472   heights. The assignments of bands are summarized in Table 1.

473   Fig. 4 Correlation between band areas of C-O (1190-845 cm^{-1}) and OH (3700-3000 cm^{-1}) within cross-sectioned

474   leaves.

475   Fig. 5 IR micro-spectroscopic mapping images of leaf sections from different heights for (a) OH band area

476   (3700-3000 cm^{-1}, abs: 0-150), (b) C-O band area (1190-845 cm^{-1}, abs: 0-50) and (c) peak height ratio of 1120

477   cm^{-1} for 1170 cm^{-1} (C-O-C bands, baseline: 1190-845 cm^{-1}, abs: 0-9). Water and polysaccharides was larger in

478   mesophyll region of 51m leaves. Change of peak height ratio with height can be tentatively explained by a

479   shift of C-O bonds by hydrogen bonding to water molecules, suggested polysaccharides may contribute to

480   water retention in upper-crown leaves around the vascular bundle and transfusion tissue.

481   Fig. 6 (a) A representative curve fitting result of OH band by four Gaussian components with initial band positions at

482   3530 (water molecules with longer H bonds), 3410 (–COOH groups in pectin-like species), 3310 (OH groups

483   in cellulose-like species) and 3210 cm^{-1} (water molecules with shorter H bonds) of a leaf at 43m. Bound water

484   might be more abundant than free water. (b) Band areas of four OH band species was larger in upper-crown

485   leaves. Error bars indicate maximum and minimum value ranges. (c) Average band area ratios (percentages in

486   the total band areas) of four OH band areas did not vary with height.

487   Fig. 7 OH and C-O band areas in mesophyll, transfusion tissue Tred vascular bundle regions extracted from the IR

488   mapping results for different heights. Different letters denote significant differences among tissues ($p < 0.05$,

489   ANOVA followed by Tukey's HSD test).

490   Fig. 8 Average band area ratios (percentages in the total band areas) of four OH species (free, pectin-like,

491   cellulose-like and bound water) for mesophyll, transfusion tissue and vascular bundle regions extracted from

492   the IR mapping results for different heights. Different letters denote significant differences among OH species

493   ($p < 0.05$, ANOVA followed by Tukey's HSD test).

494   Fig. 9 A working hypothesis for biomolecular mechanism of water retention in leaves of tall trees. (a) The carboxyl

495   groups (COOH) become deprotonated (COO-) and bound to Ca^{2+} in the cell to form Ca bridges linking pectin

496   chains. (b) Water molecules are then bound in the Ca-linked pectin molecules by hydrogen bonding to C-O-C

497   and C-OH (Modified from Fukushima et al. (2011)).

Table 1 Assignments of infrared bands observed in transmission spectra of the leaf section at 43 m (Fig.3a), in the spectra for pectin and cellulose films (Fig.3b), in the difference spectra from the 19 m spectrum for the leaves at 51, 43 and 31 m (Fig.3c) and in the OH bands of the leaves (Fig.6).

Fig. No.	Wavenumber (cm^{-1})	Assignment	Ref #
3c, 6	3530	ν(O-H) (long H bond)	8, 13
3b, 6	3410	ν(O-H) (COOH of pectin)	6
3b, 6	3310	ν(O-H) (OH of cellulose)	7, 11
3c, 6	3210	ν(O-H) (short H bond)	13, 18
3a	2920	ν_{as}(C-H) from aliphatic CH_2	2, 17
3a	2855	ν_s(C-H) from aliphatic CH_2	2, 17
3a, b, c	1740, 1735	ν(C=O) (COOH of pectin, lignin and lipids)	2, 5, 6, 9, 12, 15, 17
3a, c	1670, 1645	ν(C=O) from peptides (H-N-C=O) (amide I of proteins)	12, 14, 18
3b	1640	δ(H-O-H) of water molecules	3, 5, 10
3a, b	1610, 1625	ν(C=O) of lignin, ν_{as}(COO-) of pectin	5, 6, 12,
3a, c	1550, 1545	ν(C-N) and δ(N-H) from amide II of proteins	12, 14, 18
3c	1515	ν(C=C) of lignin	12
3b, c	1450, 1440	δ_{as}(CH_3) and δ_{as}(CH_2) of proteins, lipids and lignin	2, 12,
3a, c	1415	ν_s(COO$^-$) of pectin	5, 6, 12, 15
3b, c	1375	δ(C-H) from CH_3 groups	2, 17
3a	1370	δ_s(CH_3) and δ_s(CH_2) of proteins, lipids and lignin	12
3b	1330	ν(O-H) from COH alcohol groups of cellulose	4
3a, c	1320, 1235	ν(C-N) and δ(N-H) from amide III of proteins	12, 14
3a, b	1315	δ(O-H) in plane from alcohol groups of carbohydrates	4, 13
3c	1270	ν(C-C) and ν(C-O) of carbohydrates and lignin	12
3b, c	1170, 1150	ν_{as}(C-O-C) from glycoside of polysaccharides	1, 3, 4, 9, 13
3b	1145	ν_{as}(C-O-C) of pectin	6, 12
3c	1120	ν_{as}(C-O-C) in ring of polysaccharides	1, 3, 4
3b	1100	ν_s(COOH) of polysaccharides	10
3a, b	1020, 1030, 1050	ν(C-O) of polysaccharides and cellulose	4, 10, 13

Abbreviations designate the followings. ν_{as}: asymmetric stretch, ν_s: symmetric stretch, δ_{as}: asymmetric deformation (bend), δ_s: symmetric deformation (bend).

Band assignments are taken from references Liang and Marchessault (1959)[1], Painter et al. (1981)[2], Kačuráková et al. (1999)[3], Maréchal and Chanzy (2000)[4], Kačuráková and Wilson (2001)[5], Synytsya et al. (2003)[6], Chung et al. (2004)[7], Kubo and Kadla (2005)[8], Labbé et al. (2005)[9], , Ribeiro da Luz (2006)[10], Yang et al. (2007)[11], Heraud et al. (2007)[12], Fackler et al. (2010)[13], Fabian and Naumann (2012)[14], Szymanska-Chargot and Zdunek (2013)[15], Mayers et al. (2013)[16], Tonoue et al. (2014)[17], Kudo et al. (2017)[18].

Table 2 Results of regression analyses of IR band areas and bulk-leaf hydraulics in relation to canopy openness (O_C) and height (H).

Response variable	(a) Light only			(b) Height only			(c) Light and Height				Partial R^2 for adding:	
	β_0	β_1	R^2	β_0	β_1	R^2	β_0	β_1	β_2	R^2	Light	Height
OH band area	-47.6 *	32.1 ***	0.870	13.9	1.32 **	0.593	-43.1 **	28.2 ***	0.239	0.866	**0.273**	-0.005
C-O band area	6.09	7.72 ***	0.680	17.0 ***	0.423 ***	0.894	12.4 **	2.27	0.336 ***	0.911	0.017	**0.231**
Ψ_{sat}	-1.92 **	0.189	0.026	-1.48 ***	0.006	-0.052	-1.99 **	0.254	-0.004	-0.071	-0.020	-0.098
Ψ_{tlp}	-2.56 ***	0.143	0.142	-2.27 ***	0.005	0.049	-2.56 ***	0.144	0.000	0.047	-0.002	-0.095
RWC_{tlp}	0.57 ***	0.049 ***	0.666	0.658 ***	0.002 ***	0.629	0.60 ***	0.030	0.001	0.709	**0.080**	0.043
C_{leaf}	0.11	0.205 *	0.318	0.375 *	0.012 **	0.505	0.32	0.029	0.011	0.454	-0.051	**0.136**
WW	-0.01	0.038 *	0.395	0.062 *	0.002 *	0.322	0.01	0.027	0.001	0.354	**0.033**	-0.040
S_{leaf}	26.8	29.0 **	0.472	74.9 ***	1.39 **	0.462	41.1	16.7	0.755	0.484	**0.021**	0.011

Model equations: (a) $y = \beta_0 + \beta_1 \ln(O_C)$, (b) $y = \beta_0 + \beta_1 H$, (c) $y = \beta_0 + \beta_1 \ln(O_C) + \beta_2 H$. * $p < 0.05$, ** $p < 0.01$, *** $p < 0.001$

Table 3 Correlations of OH (3700-3000 cm^{-1}) and C-O (1190-845 cm^{-1}) IR band areas with some bulk-leaf hydraulics. Bold represents $p < 0.05$.

	Ψ_{sat}		Ψ_{tlp}		RWC_{tlp}		C_{leaf}		WW		S_{leaf}	
	R	p-value	R	p-value	R	p-value	R	p-value	R	p-value	R	p-value
OH band area	0.94	0.06	0.91	0.09	0.89	0.11	0.80	0.20	0.97	**0.03**	0.75	0.25
C-O band area	0.70	0.30	0.86	0.14	0.96	**0.04**	0.98	**0.02**	0.96	**0.04**	0.89	0.11
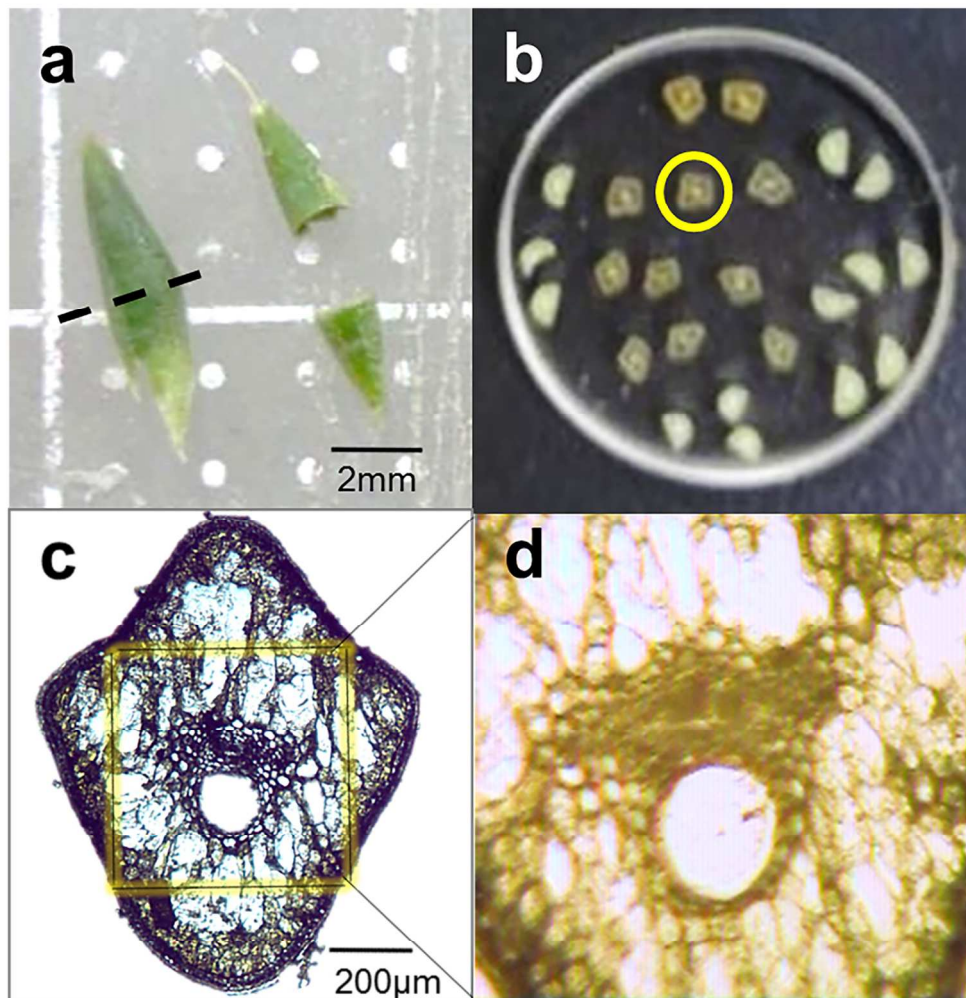
Fig. 1 Procedures for IR micro-spectroscopy of *Cryptomeria japonica* leaves.
(a) Sampling and transverse sectioning of leaves. b) Mounting of sections on CaF_2. (c) A microphoto of a transvers section. (d) A magnified central area of 625x625 μm^2 used for IR measurement.
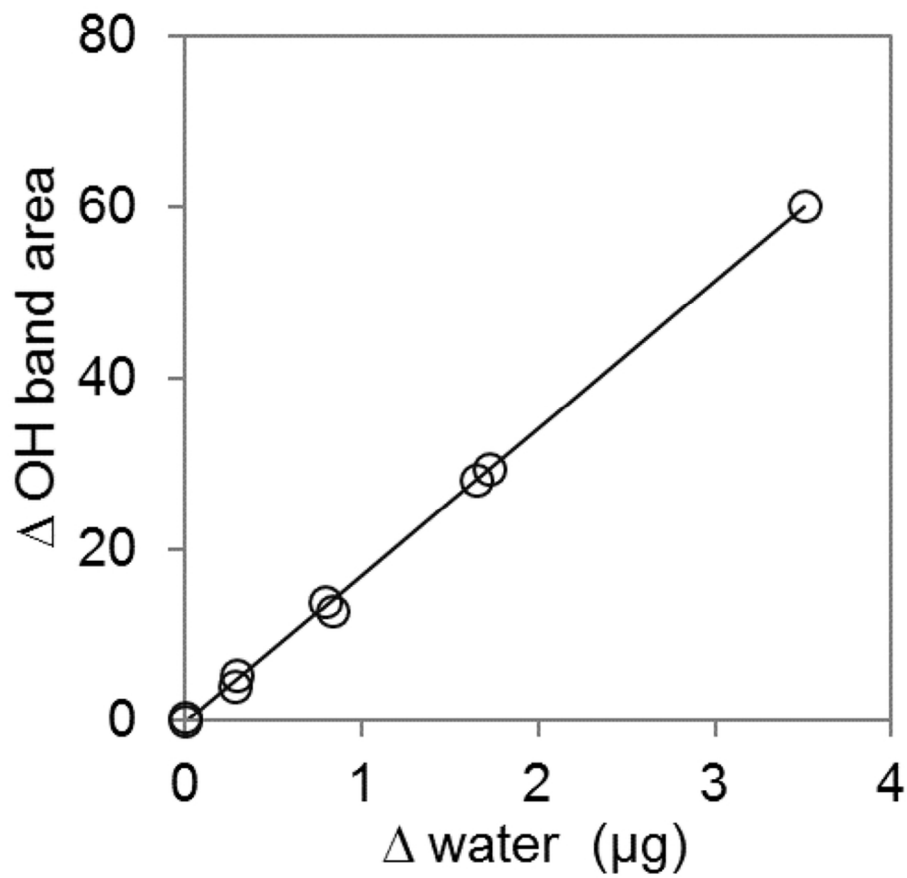
129x135mm (300 x 300 DPI)

1
2
3
4
5
6
7
8
9
10
11
12
13
14
15
16
17
18
19
20
21
22
23
24
25
26
27
28
29
30
31
32
33
34
35
36
37
38
39
40
41
42
43
44
45
46
47
48
49
50
51
52
53
54
55
56
57
58
59
60

Fig. 2 Correlation between increase in amount of water (weight increase: μg) by quartz crystal microbalance and increase in IR OH band area on a pectin film with increasing relative humidity (RH) from 20 to 30, 40, 50 and 60 %.
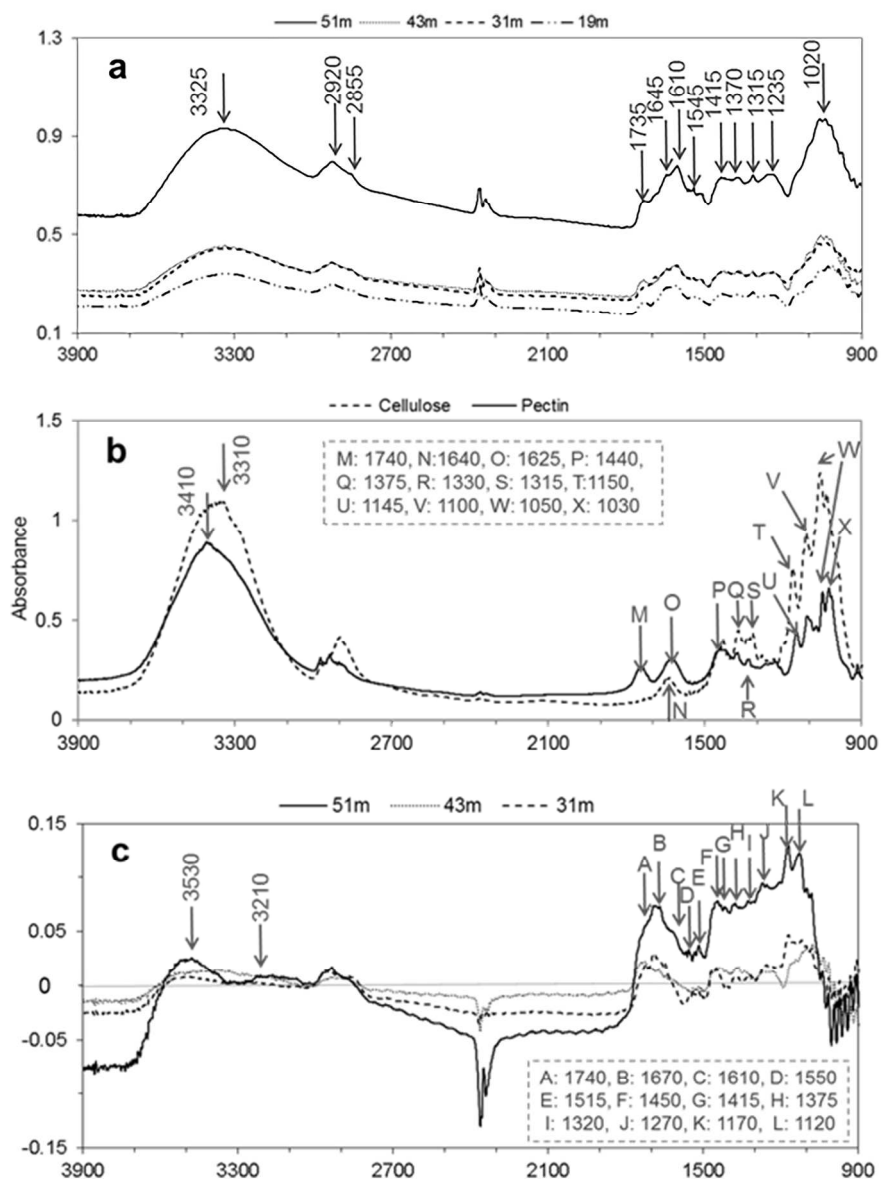
84x77mm (300 x 300 DPI)

Fig. 3 (a) IR absorbance spectra of the leaves at 19, 31, 43 and 51 m, 23 days after sectioning. (b) IR absorbance spectra of cellulose and pectin powders by KBr pellet method. (c) Difference spectra from the 19 m spectrum with a coefficient so as to obtain the absorbance zero at 3000 cm-1 (51m spectrum: 51 m – 19 m x 1.98, 43 m: 43 m – 19 m x 1.2, 31 m: 31 m – 19 m x1.33) to discriminate water and polysaccharide species at different heights. The assignments of bands are summarized in Table 1.
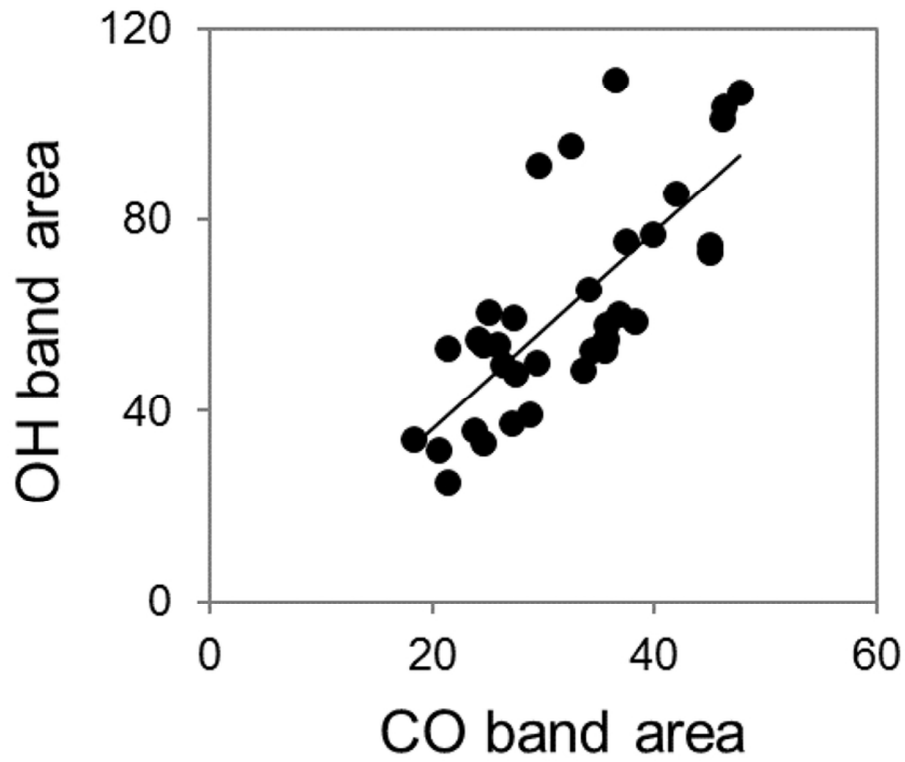
206x270mm (300 x 300 DPI)

1
2
3
4
5
6
7
8
9
10
11
12
13
14
15
16
17
18
19
20
21
22
23
24
25
26
27
28
29
30
31
32
33
34
35
36
37
38
39
40
41
42
43
44
45
46
47
48
49
50
51
52
53
54
55
56
57
58
59
60

Fig. 4 Correlation between band areas of C-O (1190-845 cm^{-1}) and OH (3700-3000 cm^{-1}) within cross-sectioned leaves.
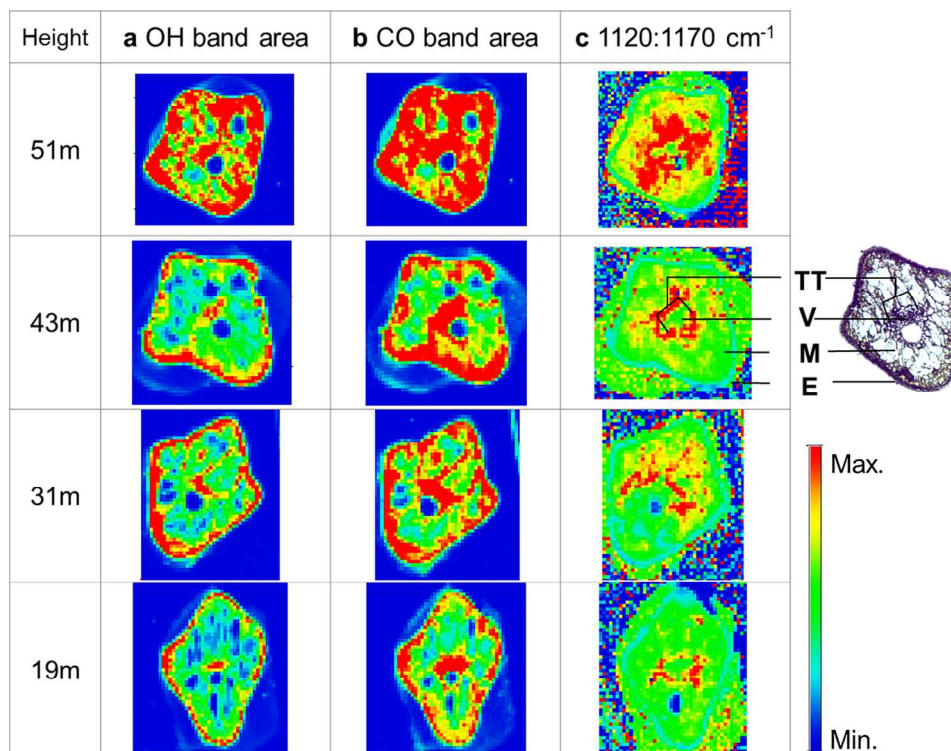
78x64mm (300 x 300 DPI)

Fig. 5 IR micro-spectroscopic mapping images of leaf sections from different heights for (a) OH band area (3700-3000 cm^{-1}, abs: 0-150), (b) C-O band area (1190-845 cm^{-1}, abs: 0-50) and (c) peak height ratio of 1120 cm^{-1} for 1170 cm^{-1} (C-O-C bands, baseline: 1190-845 cm^{-1}, abs: 0-9). Water and polysaccharides was larger in mesophyll region of 51m leaves. Change of peak height ratio with height can be tentatively explained by a shift of C-O bonds by hydrogen bonding to water molecules, suggested polysaccharides may contribute to water retention in upper-crown leaves around the vascular bundle and transfusion tissue.
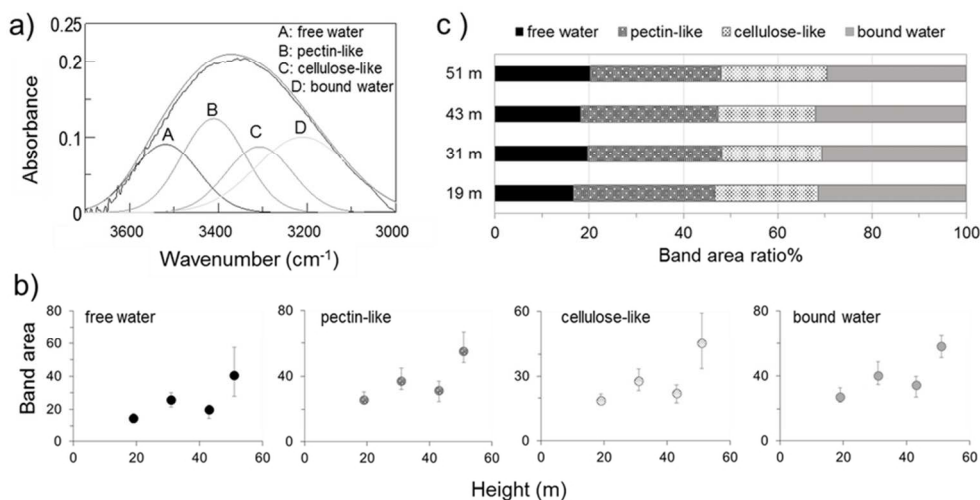
162x123mm (300 x 300 DPI)

Fig. 6 (a) A representative curve fitting result of OH band by four Gaussian components with initial band positions at 3530 (water molecules with longer H bonds), 3410 (−COOH groups in pectin-like species), 3310 (OH groups in cellulose-like species) and 3210 cm^{-1} (water molecules with shorter H bonds) of a leaf at 43m. Bound water might be more abundant than free water. (b) Band areas of four OH band species was larger in upper-crown leaves. Error bars indicate maximum and minimum value ranges. (c) Average band area ratios (percentages in the total band areas) of four OH band areas did not vary with height.
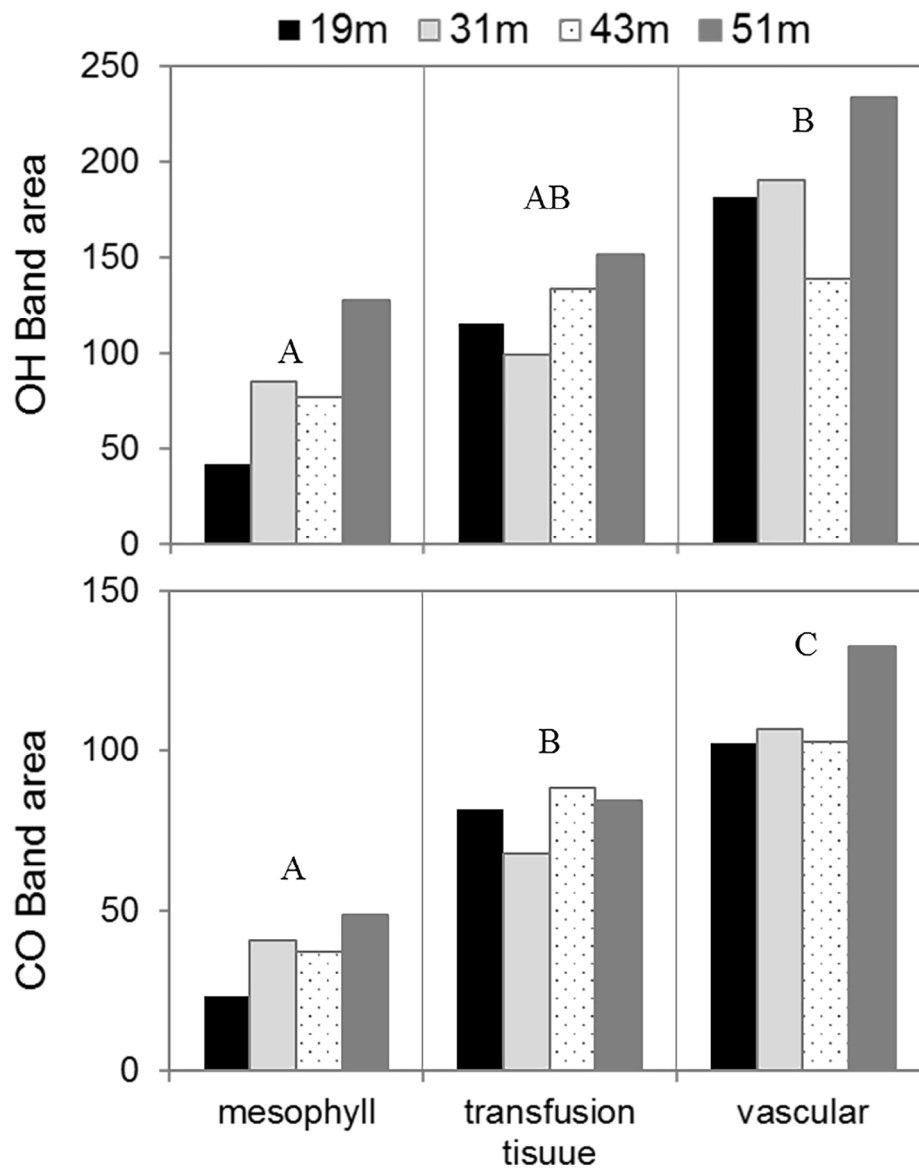
83x46mm (300 x 300 DPI)

Fig. 7 OH and C-O band areas in mesophyll, transfusion tissue and vascular bundle regions extracted from the IR mapping results for different heights. Different letters denote significant differences among tissues ($p < 0.05$, ANOVA followed by Tukey's HSD test).
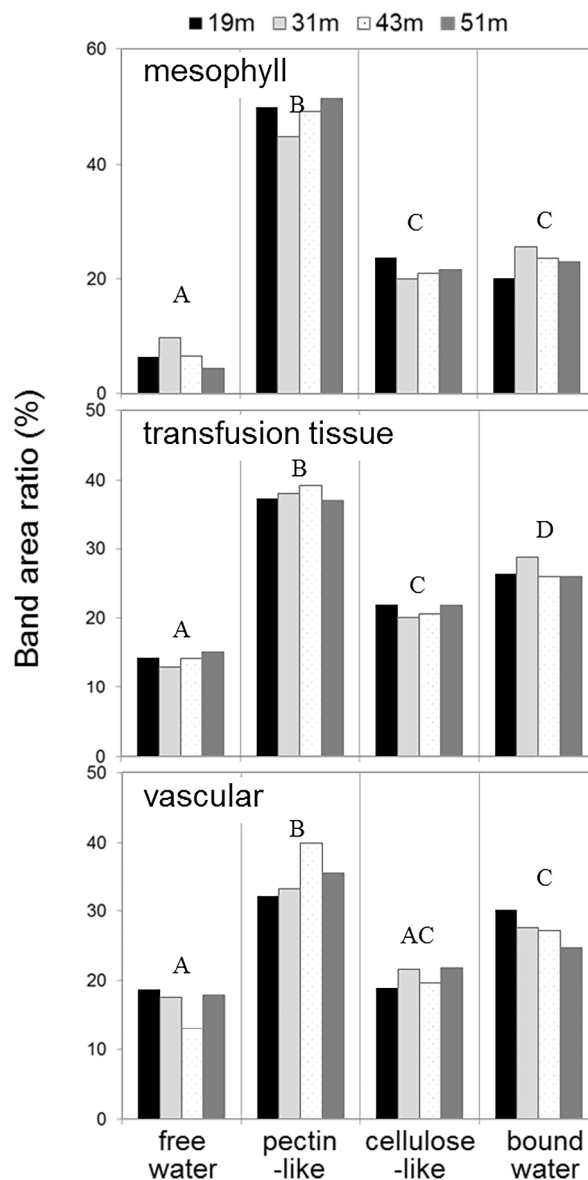
144x179mm (300 x 300 DPI)

Fig. 8 Average band area ratios (percentages in the total band areas) of four OH species (free, pectin-like, cellulose-like and bound water) for mesophyll, transfusion tissue and vascular bundle regions extracted from the IR mapping results for different heights. Different letters denote significant differences among OH species ($p < 0.05$, ANOVA followed by Tukey's HSD test).

183x357mm (300 x 300 DPI)

1
2
3
4
5
6
7
8
9
10
11
12
13
14
15
16
17
18
19
20
21
22
23
24
25
26
27
28
29
30
31
32
33
34
35
36
37
38
39
40
41
42
43
44
45
46
47
48
49
50
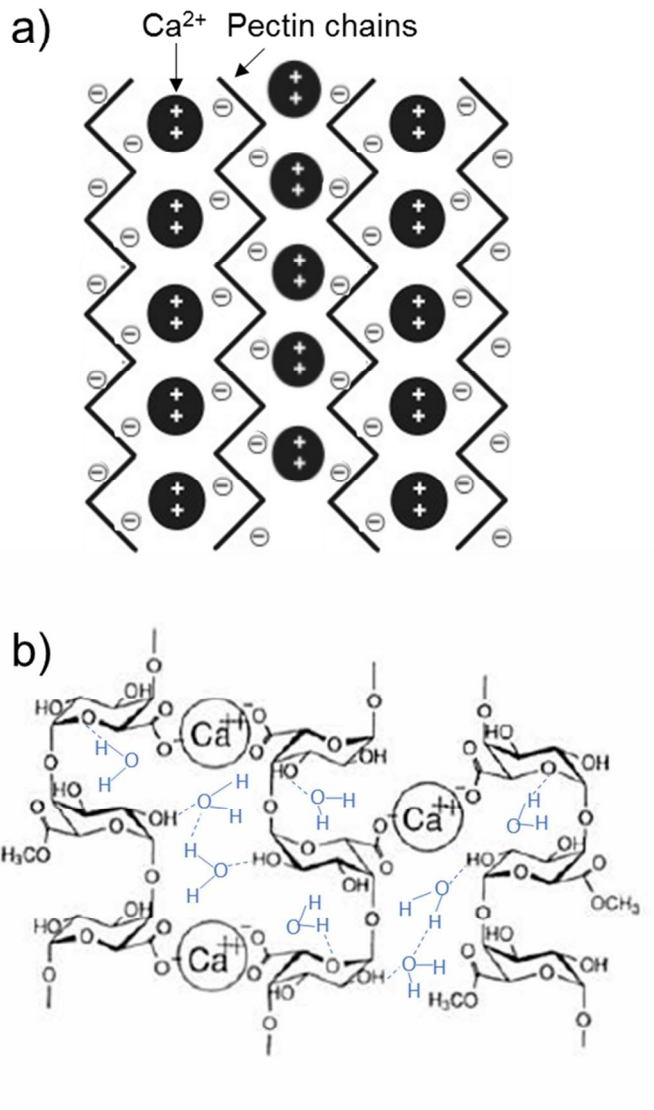51
52
53
54
55
56
57
58
59
60

Fig. 7 A working hypothesis for biomolecular mechanism of water retention in leaves of tall trees. (a) The carboxyl groups (COOH) become deprotonated (COO-) and bound to Ca^{2+} in the cell to form Ca bridges linking pectin chains. (b) Water molecules are then bound in the Ca-linked pectin molecules by hydrogen bonding to C-O-C and C-OH (Modified from Fukushima et al. (2011)).

101x125mm (300 x 300 DPI)